20. Kim, K. H.; Jun, J. H.; Lee, S. H.; Choi, J. S. *J. Phys. Chem. Solids* **1989**, *50*, 785.
21. Choi, K. M.; Kim, K. H.; Choi, J. S. *J. Phys. Chem. Solids* **1989**, *50*, 283.
22. Choi, K. M.; Kim, K. H.; Choi, J. S. *J. Phys. Chem.* **1989**, *93*, 4659.
23. Choi, K. M.; Lee, E. J.; Park, J. W.; Kim, K. H. *J. Appl. Polym. Sci.* **1991**, *42*, 2129.
24. Cho, S. K.; Kim, D.; Choi, J. S.; Kim, K. H. *J. Phys. Chem. Solids* **1989**, *51*, 113.
25. Park, J. S.; Choi, K. M.; Kim, K. H.; Choi, J. S. *J. Phys. Chem. Solids* **1989**, *50*, 903.
26. Kim, K. H.; Yun, S. H.; Choi, J. S. *J. Phys. Chem. Solids* **1989**, *50*, 291.
27. Cho, E. K.; Chung, W. Y.; Choi, K. M.; Kim, K. H. *J. Am. Ceram. Soc.* **1990**, *73*, 3470.
28. Cho, S. K.; Kim, D.; Choi, J. S.; Kim, K. H. *J. Phys. Chem. Solids* **1989**, *51*, 113.
29. Kim, K. H.; Huong, P. V.; Oh-Kim, E.; Lalhaye, M.; Cho, S. K.; Kwak, B. C. *J. Less-Comm. Met.* **1990**, *164*, 1201.
30. Shaplygin, I. S.; Lazarev, V. B.; Russ, *J. Inorg. Chem.* **1985**, *30*, 1828.
31. Nakamura, T.; Misono, M.; Yoneda, Y. *J. Catal.* **1983**, *83*, 151.

Direct Solid Sample Analysis in the Moderate Power He Mip with the Spark Generation

S. R. Koirtyohann* and Yong-Nam Pak†

**Department of Chemistry, Univeristy of Missouri, Columbia, MO 65201, U.S.A.*
†*Department of Chemistry Education, Korea National University of Eduction, Cheong-Won, 363-791, Korea*
Received March 11, 1994

Conducting solid samples are successfully analyzed with the spark ablation combined to the moderate power (500 W) Helium Microwave Induced Plasma (He MIP). The relative standard deviations are in the range of 3-10% and the detection limits are around 50 μg g^{-1}. These values are higher than those of Ar MIP or Ar Inductively Coupled Plasma. Spark ablated particles are examined to investigate the analytical characteristics of the system.

Introduction

It is more advantageous analyzing a solid sample directly rather than dissolving it because of the time to dissolve and the risk of contamination from the chemicals used in the dissolution step. Also, the direct solid sample analysis should be inherently more sensitive when it is considered that only 1-2% of the total solution is delivered into the atomizer and the rest to a waste bottle. Thus, Arc/spark discharges have been used for the ICP[1-6] (Inductively Coupled Plasma) for conducting solid sample analysis.

Recent developments in the moderate power (up to 500 W) Helium and Argon Microwave Induced Plasmas (MIPs) have allowed them to be utilized in many spectroscopic areas[7-14] including MIP/Mass Spectrometry[12-14]. Their applications are well described in the review[15]. The Ar MIP has been used for metals while the He MIP has exclusively been used for non-metals such as halogens due to its high ionization potential available. The Ar plasma which has a desirable annular shape showed good analytical performances. The moderate power Ar MIP[10,11] gave good sensitivities and large dynamic ranges for metal ions even in aqueous samples of complex matrix.

On the other hand, the He MIP has been used mostly for the gaseous samples because of its low kinetic temperature[16]. Even the moderate power He MIP has shown insufficient vaporization of the samples and consequently, more interferences and worse detection limits[8] than the Ar MIP. One reason is that a He plasma forms a cylindrical shape instead of a toroidal one. Thus, samples do not penetrate the hottest core of the plasma and show large interferences. In addition to that, the temperature and electron number density (T_{rot}=2,500 K and 2.1×10^{14}/cm^3) indicate[17] that the moderate power He MIP is not sufficiently "hot" in handling aqueous samples. However, the very high ionization temperature[17] of the He MIP provides its unusually high excitation capability.

In order to employ this efficient excitation character of a He plasma exclusively, "dried" particles are generated by the spark and introduced to the system. Since early works on the low power (100 W) He MIP with gaseous samples have been successful, it is expected that the "dried" particles introduced to the moderate power MIP should give good analytical results. Increasing power to a moderate level (up to 500 W) also should be a factor beneficial to the solid sample analysis. One of the purpose of this research is to examine the usefulness of the moderate power He MIP upon the introduction of "dried" particles. Analytical characteristics of the moderate power Spark/He MIP system will be compared with those of the Spark/Ar MIP system[18].

Experiment

Instrumentation

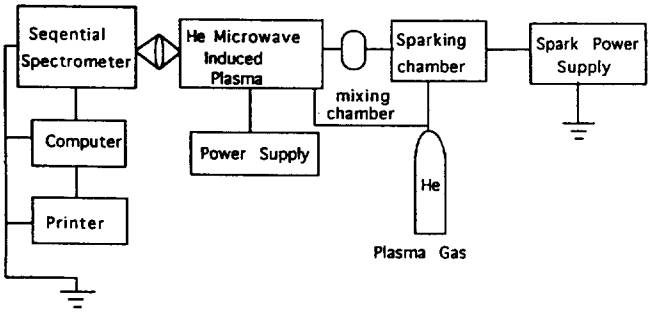

Figure 1. A block diagram of experimental set-up.

The experimental system is shown in Figure 1. A detailed explanation on the experimental system is given in the previous literature[18]. The He plasma was sustained in a modified TM_{010} resonant cavity operated at 475 W forward power. Reflected power was kept minimum (less than 5 W) by reading the meter at the generator. Because of the power loss to the tuning stubs and transmission cable, the real power coupled to the plasma was less than 500 W. The modified TM_{010} cavity used internal tuning[19] stubs. The cavity was installed in a commercial ICP unit (Perkin Elmer 6500) modified to perform the direct solid sample analysis. The spectrometer was a sequential slew scanning type and an unidirectional spark power source was employed.

Reagents and Samples

The samples used in this study were conducting metals such as NIST-SRM low alloy steel (from 1261a-1264a) and Al (601-604 and 7075). The counter electrode used in the spark was a graphite rod of spectroscopic grade (Union Carbide, Sommerville, N. J.). The He gas used was 99.995% pure.

Particles generated by the He spark were examined by Scanning Electron Microscopy (SEM). The total amount of particles was determined by collecting the particles using 0.20 μm pore cellulose acetate filters (Model GS, Millipore Corporation, Bedford, Massachusetts) in the transport line. The filter and support pads were placed in a sample holder (MSA #46, Model AP10, Montitaire, Pittsburgh, Pennsylvania).

Procedures

After 20 minutes of warming-up for the He MIP, a conductive sample of which surface had been smoothed and cleaned was sparked in the sampling chamber for 3 minutes. Thirty seconds were allowed for the prespark so that the signal was to be equilibrated. Up to 18 elements could be analyzed for the remaining 150 seconds. In particle study, particles were collected from the trap installed just before the plasma. After 30 burns, filters were collected and dissolved in conc. HCl, boiled until the solution was almost dried. Then it was diluted with water to 30 *ml*. The solution was analyzed by the ICP-AES.

Optimization

Plasma. The optimum conditions for the He spark-He MIP are shown in Table 1 and they are different from those of the Ar spark-Ar MIP system. Power and tangential gas flow were studied. The other conditions were selected based on the MIP-AES study. When Al (392.6 nm) was analyzed, signal-to-noise (S/N) ratio increased with the power increase (Figure 2). Noise was evaluated by measuring the peak to peak height in the background while no sample was sent. Though the maximum power was 500 W, 475 W was used in order to monitor any power change during a run. The plasma (or tangential) gas flow was optimized to be 5.0 L /min. Below this flow, the plasma torch was easily deteriorated. Higher flows only reduced the signal as shown in Figure 3.

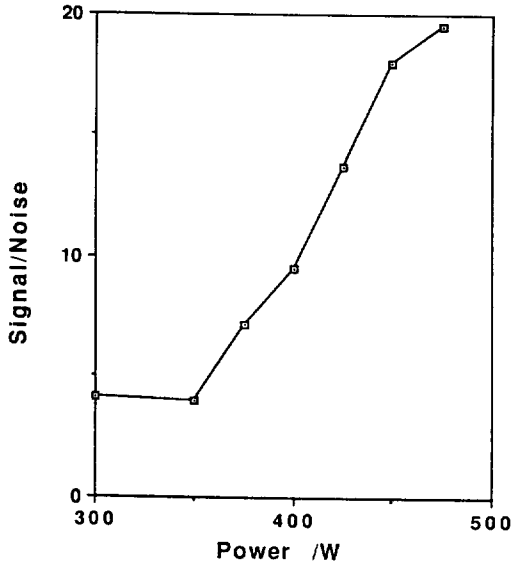

Figure 2. Signal to noise ratio as a function of power. Al 392.6 nm was monitored for aluminum alloy.

Table 1. Optimum Operating Conditions for the He Spark-MIP

Plasma conditions	
Plasma He flow rate	5.0 L/min
Sample He flow rate	1.1 L/min
Power, forward	475 W
Power, reflected	<5 W
Integration time	5 sec.
Spark conditions	
Inductance	40 μH
Capacitance	2.5 nF
Breaks per half cycle	2
Analytical gap distance	4 mm*, 3 mm+
Variac power setting	30
Breakdown voltage	10.6 kV
Prespark	30 sec.

*for low alloy steel. +for Al alloy.

Spark. The analytical gap distance was examined first. Because if the current is determined by the distance between the sample and the counter electrode, then a sample determines the sampling efficiency. To avoid this situation, the auxiliary gap distance is determined for the given break down voltage of 10.6 kV. The analytical gap distance greater

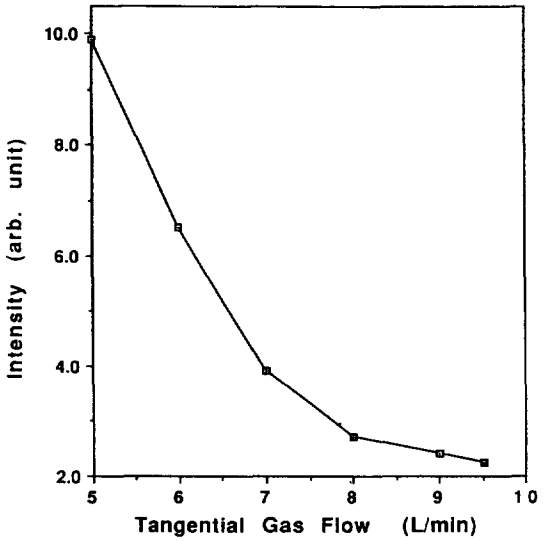

Figure 3. Intensity as a function of the plasma tangential gas flow. Al 396.2 nm was selected in Al alloy.

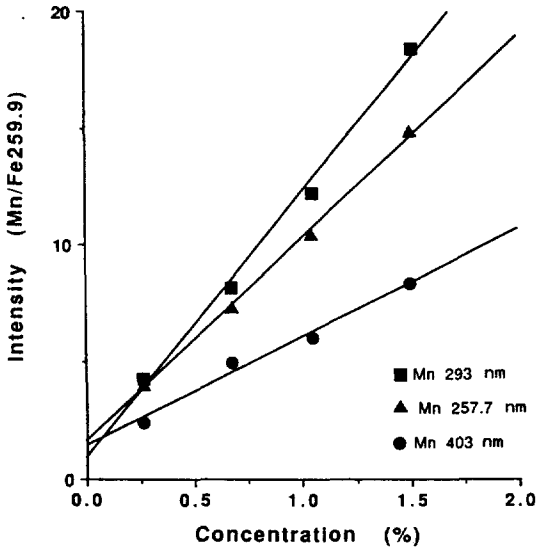

Figure 4. Calibration curves of low alloy steels for different Mn transitions in the spark-He MIP.

Table 2. Comparison of S/B Ratios for Two Sample Gas Configurations with Low Alloy Steel and Aluminum in the He Spark-MIP

Element	line (nm)	Configuration Tangential (S/B)	Gas sweep (S/B)
Low alloy steel			
Ni	221.6	5.8(4.9/.85)	0.78(2.5/3.2)
Mn	259.3	8.3(82.7/10)	9.1 (118/13)
Cr	267.7	9.1(18.2/2.0)	8.8 (11.5/1.3)
Al	396.2	4.3(61/14.3)	1.5 (8.5/5.6)
Cu	224.7	7.9(165/21)	6.4 (115/18)
Aluminum alloy			
Ni	221.6	54 (172/3.2)	7.5 (75.1/10)
Mn	259.3	21 (135/6.4)	3.6 (54/15)
Cr	267.7	4.4(78.5/18)	2.0 (47.3/25)
Zn	213.9	11 (108/9.8)	12 (78.7/5.0)
Mg	279.5	150 (460/3.0)	28 (110/4.0)
Cu	324.75	34.5(200/5.8)	33 (110/3.3)

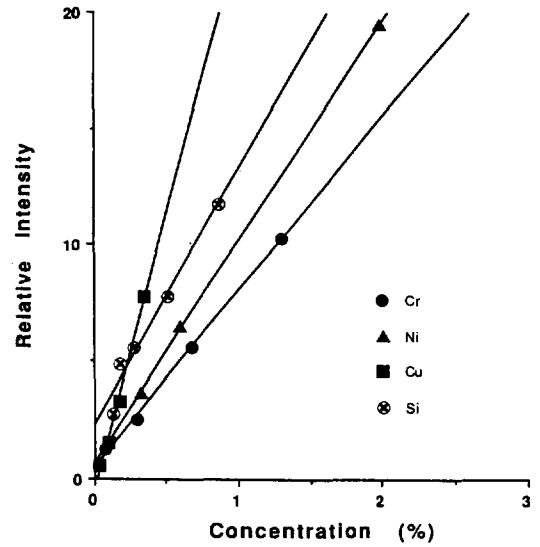

Figure 5. Calibration curves of several elements in low alloy steel (except Si in aluminum) in the He spark-MIP.

than 5 mm drops the S/N ratio significantly (more than 50%). Performance was relatively independent of the gap distance so long as it was 4 mm or less for low alloy steel. For Al alloy, 3 mm was chosen because it gave slightly better performance over 4 mm.

When the number of breaks per half cycle (BHC) was increased, the intensity was increased. However, the plasma frequently arced down to the tip of PTFE thread as more particles were introduced. For this reason, 2 BHC is used throughout the experiment and a better reproducibility is obtained. Capacitance was fixed at 2.5 nF at the above conditions for similar reasons. When the capacitance was increased, the power was needed to be increased to maintain 2 BHC and consequently caused the problem of arcing.

Sample Gas Configuration. The sample gas could be sent through the tangential arm of the sparking chamber (tangential configuration) or through the electrode (gas sweep configuration). Both configurations were examined with the use of S/B ratio. Backgrounds were measured near or at the analytical lines while the spark was operating. Table 2 lists the S/B ratio of two sample gas configurations for the low alloy steel and aluminum alloy. The tangential configuration gave higher signal and background intensities than the gas sweep configuration for most of elements examined. The S/B ratios of the tangential configuration were similar or better for all of the elements. The noises in the background were about the same for both configurations.

Results and Discussion

Analytical Performances of the Spark He-MIP System. Figure 4 shows the calibration curve for different

Table 3. The List of Relative Standard Deviation (RSD) of Low Alloy Steel and Aluminum in the He Spark-MIP (tangential, sample 1263, 601)

Element	Line (nm)	Conc. (%)	RSD (%)
Low Alloy Steel			
Ni	221.65	.32	6.4
Cu	224.7	.098	6.3
Co	228.6	.15	2.7
Cr	267.7	.30	2.8
Al	396.15	.24	9.8
Mn	257.6	.258	3.1
Si	251.6	.74	4.1
Aluminum alloy			
Fe	238.2	.52	11.1
Cu	324.75	4.38	3.1
Mg	279.55	1.56	9.9
Mn	257.6	.81	6.3
Ni	213.86	.06	35

energy transitions of Mn. Intensity ratios of Mn lines to Fe 259.9 nm are plotted with respect to % concentration. It is demonstrated here that the He MIP is capable of exciting all levels of Mn yielding good linearity. Calibration curves for other elements shown in Figure 5 also reveal that the spark-He MIP system is performing well. All calibration curves were linear over the range of concentrations found in the samples. The largest range available was for Cr where linearity over 2 orders of magnitude was demonstrated. The lower and upper limits of the range were limited by the sample available rather than the system. In all transitions, Fe 259.9 nm was used as an internal standard. When a different internal standard line such as Fe 238.2 nm was used, there was no difference in the linearity compared to Fe 259.9 nm. Most of curves pass through or near the origin except for Si. Though background was automatically corrected by subtracting the intensity at the vicinity of the analytical line, this can not solve all problems if the background is strongly featured. Most of sensitive Si lines have some featured background. Another reason why Si does not have zero intercept could be the bleeding from the quartz torch made of SiO_2.

The RSDs between the runs and the line used are listed in Table 3. For low alloy steels, they are around 3-10%. Aluminum alloy samples show higher RSD with 5 or 6 observations. When a line ratio (using Fe as an internal standard) was used, the RSD values were almost the same or even worse in some occasions. It is suspected that the noise within a run is larger than the fluctuations between the runs. Nevertheless, should there be occasional spikes during the experiments, internal standard was used to prevent any error due to sudden changes. In order to improve the RSD, noise within a run must be reduced first as well as between the runs. Two most significant noise sources are spark discharge wander and fractional distillation. Wander of the sampling spot over the sample surface results in flicker noise in the analytical signal.

Signal to noise ratios (S/N) and detection limits are calculated and listed in Table 4. S/N was calculated for a given concentration and extrapolated, assuming constant noise, to where signal is three times larger than noise which is the standard deviation of background. The concentration at which S/N becomes 3 is the detection limit (DL). A typical DL is around 50 μg g^{-1} in the spark-He MIP.

Table 4. The Detection Limits for the He Spark-MIP

Element	Line (nm)	Conc. (%)	S/B	S/N	Detection limit (%)
Cr	267.7	0.69	3.3	590	.0035
Ni	227.2	0.60	2.3	390	.0046
Mn	257.6	0.67	18	460	.0044
Cu	224.7	0.51	.9	110	.0146
Al	396.15	0.095	1.4	51	.0056
Si	251.6	0.4	4	430	.0028

Table 5. List of Correlation Coefficients of the He Spark-MIP

Element	Correlation coefficient (r)
Mn	0.9985± 0.0005
Cr	0.9995± 0.0003
Co	0.9980± 0.0020
Al	0.9995± 0.0005
Ni	0.9982± 0.0024
Cu*	0.9941± 0.0056

Cu* is from aluminum alloy.

The performance of the He MIP in solid sample analysis is also shown in Table 5, where correlation coefficients (r) for low alloy steel and Aluminum are listed. The r values listed are between 0.9941 and 0.9995. The moderate power He spark-MIP are much better than the low power He spark-MIP done by Walter[20] (r values around 0.98 or less).

Compared to the Ar spark-MIP, the He spark-MIP gives worse detection limits of about an order of magnitude. The r values of the spark He-MIP are somewhat worse than those of spark-Ar MIP[18] or Ar ICP system[21]. In precision, they are similar for the low alloy steel but the He spark-MIP gives better RSD values for aluminum alloy. Overall, the analytical ability of the He spark-MIP is less than that of the spark-Ar MIP. The differences between them are due to the facts that; first, the plasmas are quite dissimilar in shape, causing differences in sample mixing with the plasma. Ar plasma forms the desirable annular shape so that samples could mix well. Secondly, the spark sampling efficiency also varies with the type of sample gas used. The Ar spark produces more of small particles than the He spark does[21]. Finally, Ar MIP is thermally hotter than He MIP, vaporizing particles more efficiently.

Transport Rate and Particle Studies. The transport rate was examined by collecting ablated particles from the trap installed just before the plasma. The total transport rate with different gases as well as different sample configurations are compared in Table 6. Several major elements could be used to calculate the total transport rate. There are dissimilarities in the transport rate values among the elements

Table 6. The Transport Rates of Low Alloy Steel Samples with Different Sample Gas Configurations in He and Ar Sparks

Element used for calculation		Tangential μg sec^{-1}	Gas sweep μg sec^{-1}
He spark	Fe	0.33	0.27
	Mn	0.40	0.30
	Cr	0.48	0.36
Ar spark	Fe	0.22*	0.50*
	Mn	0.23	

*from ref. 21.

used, though the trend does not change between the sample gas modes regardless of the element chosen. Since Fe is the major element, it should contain the least error. One point to be noticed in this study is that the total transport rate varies with the sample gas mode used. In He gas, more particles are generated in the tangential mode. On the contrary, in the Ar spark, the gas sweep mode produced about twice as much as the tangential mode. Overall, the Ar spark generated more particles than the He spark. These results are consistent with the S/B study discussed earlier. One of the reasons why the Ar spark-MIP shows lower detection limits than those of the He spark-MIP is that the Ar spark produce more particles.

Particle study done by Prell[21] in the Spark-ICP showed that the gas sweep configuration has better S/N and RSD, that is observed also in the Ar spark-MIP. However, in the He spark-MIP, the tangential mode produced better results (Table 2). In order to understand this opposite behavior, particles generated under different gases were collected and examined with the SEM. Two groups of different particles are observed (Figure 6). Walters *et al.*[22] used a light scattering technique to probe the spatial and temporal behavior of particles in the Ar spark. Their study demonstrated the presence of small particles (0.1-1 μm) as well as large particles (>2 μm). The two types of particles were believed to have very different histories, with the large spheres representing solidified liquid droplets and that the small particles were from condensed free atoms, which later coalesced into clusters. Ekimoff and Walter[23] found two distinctive types of particles, which were related to the analytical performance. Prell[21] argued that the shape of particles generated is directly related to the analytical performance of spark-plasma system. That is, small particles play a more beneficial role.

In the Ar spark, the gas sweep configuration not only makes more sample particles but it generates more small particles which yields better performance. On the other hand, in the He spark, more of small particles (<1 μm) are generated in the tangential configuration and yields better performance.

The solid aerosol sample introduction method could offer advantages over dissolution method, one of which is enhanced sensitivity. To compare the direct solid aerosol introduction with a solution nebulization, the minimum detectable transport rate is calculated. The measured detection limit of Mn in the He spark-MIP is 44 μg g^{-1}, which is 0.013 ng s^{-1} in terms of transport rate. When the detection limit of Mn in aqueous sample is considered as 100 ppb, the transport rate for DL is 0.10 ng s^{-1}. The use of spark-MIP, which introduces dried samples, demonstrates about an order of magnitude improvement in absolute detection limit. Spark ablated sample introduction could offer two advantages. One is to introduce more sample in an atomizer. The other is to bring desolvated ones, thus increasing excitation efficiency especially important in the He MIP.

(a)

(b)

Figure 6. Micrographs of particles collected under the He spark. (a) Large particle of which diameter is about 10 μm. This type of particles are more found in the gas sweep mode. (b) Small particle of which diameter is less than 1 μm. These particles are found in the tangential gas mode more.

Conclusion

The moderate power He MIP has been used successfully for the analysis of metal samples with the combination of the spark. The optimum conditions of the Spark/He MIP system were sought and its analytical performances were evaluated. The detection limits are around 50 μg g^{-1} for low alloy steels and aluminum samples with the RSD of less than 10% mostly. The RSD and detection limits are worse than those of the spark-Ar MIP because of less ablated particles generated and the characteristics of the plasma. Compared to the Ar MIP, studies thus far indicate that the He MIP is not thermally "hot" enough to vaporize and efficiently

excite metal particles.

However, it can provide an efficient method for the direct analysis of conducting samples and the moderate power system performs better than the low power. A simple calculation reveals that dried solid aerosol introduction is one order of magnitude more sensitive than the aqueous sample introduction.

References

1. Codeo, A. G.; Lopez, M. T. D.; Seco, J. L. J.; Cobo, I. *J. Anal. At. Spectrom.* **1992**, *7*, 11.
2. Ono, A.; Saeki, A.; Chiba, K. *Appl. Spectrosc.* **1987**, *41*, 970.
3. Marks, J. Y.; Fornwalt, D. E.; Yungk, D. E. *Spectrochim. Acta. Part B* **1983**, *83*, 107.
4. Human, H. G. C.; Scott, R. H.; Oakes, A. R.; West, C. D. *Analyst* **1976**, *101*, 265.
5. Aziz, A.; Broekaert, J. A. C.; Laqua, K.; Leis, F. *Spectrochim. Acta. Part B* **1984**, *39*, 1091.
6. Marks, J. Y.; Fornwalt, D. E.; Yungk, R. E. *Spectrochim. Acta. Part B* **1983**, *38*, 107.
7. Zhang, L.; Carnahan, J. W.; Winans, R. E.; Neil, P. H. *Anal. Chem.* **1991**, *63*, 212.
8. Michlewicz, K. G.; Carnahan, J. W. *Anal. Chem.* **1986**, *58*, 3122.
9. Ng, K. C.; Shen, W. *Anal. Chem.* **1986**, *58*, 2084.
10. Brown, P. G.; Haas, D. L.; Workman, J. M.; Caruso, J. A.; Fricke, F. L. *Anal. Chem.* **1987**, *59*, 1433.
11. Haas, D. L.; Caruso, J. A. *Anal. Chem.* **1984**, *56*, 2014.
12. Wilson, D. A.; Vickers, G. H.; Hieftje, G. M. *Anal. Chem.* **1987**, *59*, 1661.
13. Creed, J. T.; Davidson, T. M.; Shen, W.; Brown, P. G.; Caruso, J. A. *Spectrochim. Acta, Part B* **1989**, *44*, 909.
14. Park, C. J.; Pak, Y. N.; Lee, K. W. *Anal. Sci.* **1992**, *8*, 443.
15. Gustavsson, A. G. T. In *Inductively Coupled Plasmas in Analytical Atomic Spectrometry*; Montaser, A.; Golightly, D. W., Ed.; VCH Publishers, New York, U. S. A. 1987; p 399.
16. Zander, A. T.; Hieftje, G. M. *Anal. Chem.* **1978**, *50*, 1257.
17. Pak, Y. N.; Koirtyohann, S. R. *Submitted to Spectrochim. Acta, Part B.*
18. Pak, Y. N.; Koirtyohann, S. R. *Submitted to J. Anal. At. Spectrom..*
19. Haas, D. L.; Carnahan, J. W.; Caruso, J. A. *Appl. Spectrosc.* **1983**, *37*, 82.
20. Helmer, D.; Walters, J. P. *Appl. Spectrosc.* **1984**, *38*, 399.
21. Prell, L.; Koirtyohann, S. R. *Appl. Spectrosc.* **1988**, *42*, 1221.
22. Scheeline, A.; Norris, J. A.; Travis, J. C.; Devope, J. R.; Walters, J. P. *Spectrochim. Acta, Part B* **1981**, *36*, 373.
23. Ekimoff, D.; Walters, J. P. *Anal. Chem.* **1981**, *53*, 1644.

On the Stationary Probability Distributions for the Schlögl Model with the First Order Transition under the Influence of Singular Multiplicative Noise

Kyoung-Ran Kim, Dong J. Lee, Cheol-Ju Kim*, and Kook Joe Shin**

Department of Chemistry, National Fisheries University of Pusan, Pusan 608-737, Korea
**Department of Chemistry, Chonbuk National University, Chonbuk 560-742, Korea*
***Department of Chemistry, Seoul National University, Seoul 151-742, Korea*

Received March 21, 1994

For the Schlögl model with the first order transition under the influence of the multiplicative noise singular at the unstable steady state, the effects of the parameters on the stationary pobability distributions obtained by the Ito and Stratonovich methods are discussed and compared in detail.

Introduction

Recently, much attention has been paid to the stochastic processes with multiplicative random force in the fields of theoretical physics and chemistry.[1-5] Two of us[5] have discussed the stochastic phenomena for the Schlögl model with the first order transition driven by the multiplicative random force singular at the unstable steady state. The effects of the singularity on the stationary probability distribution based on the Stratonovich theory have been analyzed in detail. Then, the transition rate has been discussed from one stable steady state to the other stable steady state through the unstable steady state.

The Schlögl model exhibiting the first order transition in chemical reaction is given by[5-7]

$$A \xrightarrow{k_1} X,\ B+X \underset{k_{-2}}{\overset{k_2}{\rightleftarrows}} 3X+C,\ D+X \xrightarrow{k_3} E, \tag{1}$$

where k_i's are the rate constants, A, B and D are the concentrations of reactants and C and E denote those of products. The rate equation for X is given by the following equation while concentrations of other species being held constant